PCCP

Physical Chemistry Chemical Physics

Accepted Manuscript

This article can be cited before page numbers have been issued, to do this please use: S. Aparicio, M. Atilhan, A. Gutierrez, S. Martel, J. A. Tamayo, R. Barros, A. Bol, F. C. Gennari and P. Arneodo Larochette, *Phys. Chem. Chem. Phys.*, 2022, DOI: 10.1039/D2CP00346E.

View Article Online
DOI: 10.1039/D2CP00346E

A theoretical study on CO_2 at Li_4SiO_4 and Li_3NaSiO_4 surfaces

Alberto Gutiérrez,[a,b] Juan Antonio Tamayo-Ramos,[b] Sonia Martel,[b] Rocío Barros,[b] Alfredo Bol,[b,c] Fabiana Cristina Gennari,[d,e] Pierre Arneodo Larochette,[d,e] Mert Atilhan,[f] Santiago Aparicio*[a,b]

[a] Department of Chemistry, University of Burgos, 09001, Burgos, Spain

[b] International Research Center in Critical Raw Materials for Advanced Industrial Technologies (ICCRAM), University of Burgos, 09001 Burgos, Spain

[c] Department of Physics, University of Burgos, 09001 Burgos, Spain

[d] National Scientific and Technical Research Council (CONICET), Bariloche Atomic Centre (CNEA), R8402AGP, S. C. de Bariloche, Río Negro, Argentina

[f] Department of Chemical and Paper Enginering, Western Michigan University, Kalamazoo MI 49008-5462 USA

[e] Balseiro Institute (National University of Cuyo), R8402AGP, S. C. de Bariloche, Río Negro, Argentina

*Corresponding authors: sapar@ubu.es

ABSTRACT: Lithium silicates have attracted great attention in recent years due to their potential use as high-temperature (450-700 °C) sorbents for CO_2 capture. Lithium orthosilicate (Li_4SiO_4) can theoretically adsorb CO_2 in amounts up to 0.36 g CO_2/g Li_4SiO_4. The development of new Li_4SiO_4-based sorbents is hindered by a lack of knowledge of the mechanisms ruling CO_2 adsorption on the Li_4SiO_4, especially for eutectic mixtures. In this work, the structural, electronic, thermodynamic and CO_2 capture properties of monoclinic phases of Li_4SiO_4 and a binary (Li_3NaSiO_4) eutectic mixture are investigated using Density Functional Theory. The properties of the bulk crystal phases as well as of the relevant surfaces are analysed. Likewise, the results for CO_2 – lithium silicates indicate that CO_2 is strongly adsorbed on the oxygen sites of both sorbents through chemisorption, causing an alteration not only in the chemical structure and atomic charges of the gas, as reflected by both the angles and bond distances as well as atomic charges, but also in the cell parameters of the Li_4SiO_4 and Li_3NaSiO_4 systems, especially in Li_4SiO_4 (001) and Li_3NaSiO_4 (010) surfaces. The results confirm strong adsorption of CO_2 molecules on all the considered surfaces and materials followed by CO_2 activation as inferred from CO_2 bending, bond elongation and surface to CO2 charge transfer, indicated CO_2 chemisorption for all the cases. The Li_4SiO_4 and Li_3NaSiO_4 surfaces may be proposed as suitable sorbents for CO2 capturing in wide temperature ranges.

View Article Online
DOI: 10.1039/D2CP00346E

1 Introduction

In the last decades, a significant increase level of atmospheric carbon dioxide (CO_2), which has been identified as the most important contributor to global warming, has taken place. CO_2 concentration in the atmosphere recently exceeded the threshold of 400 ppm, [1] and the increasing trend does not appear to slow down. The main source of CO_2 is fossil fuels burning for energy production,[2] so there is an urgent need to develop cost-effective and environmentally acceptable CO_2-capturing technologies[3,4] in order to reduce emissions. Concretely, high-temperature adsorption using solid sorbents is an attractive CO_2 capture option because a lot of energy can be saved during the process by recycling the heat emitted from the exothermic adsorption of CO_2 by the solid sorbents in the reactor.

The analysis of surface properties in terms of CO_2 activation via adsorption is of great relevance for understanding the CO_2 capturing mechanism and energetics in solid sorbent. The adsorption and activation on different surfaces is confirmed by large adsorption energies,[5] bending of CO_2 molecules,[6] charge transfer from the surface to the gas molecule and even breaking of CO_2 molecules in some cases.[7] All these parameters are used to quantify the extension of CO_2 activation and thus the possible chemisorption on the surface.

Among the various solid sorbents that have been investigated and proposed in literature, CaO- and Li_2O-based sorbents, as well as hydrotalcite, are the most studied high-temperature sorbents.[8] Hydrotalcites have lower CO_2 adsorption capacity (0.029 $g_{gas}{\cdot}g^{-1}_{sorbent}$) [9] than CaO- and Li_2O-based sorbents (0.79 $g_{gas}{\cdot}g^{-1}_{sorbent}$ and 0.36 $g_{gas}{\cdot}g^{-1}_{sorbent}$ respectively),[10,11,12] so they are less used in carbon capture. Among the other sorbents, Li_2O-based ones are more desirable because its regeneration does not consume as much energy as CaO-based ones, which is normally operated at 900 °C in practical applications.[13] Lithium containing materials such as lithium zirconate (Li_2ZrO_3) and lithium orthosilicate (Li_4SiO_4) seem to be promising CO_2 acceptors in the 500-700 °C range. These silicates show fast adsorption rates, high capture capability, and good durability of repeated adsorption-desorption cycles.[14,15] Specifically, Li_4SiO_4 is considered as one of the most promising candidates at high temperature and low concentrations because it has 30 times faster CO_2 adsorption (at the same sorption

View Article Online
DOI: 10.1039/D2CP00346E

conditions) and lower cost of the raw materials involved than Li_2ZrO_3.[16] However, it usually suffers from slow kinetics at low CO_2 concentrations, so an effective way to enhance the kinetics of pure Li_4SiO_4 is to dope it with heteroatoms such as Na,[17,18] K, [19,20] Al [21] or Fe.[22]

The CO_2 adsorption behaviour of Li_4SiO_4-based sorbents has been studied in the literature at low temperatures,[23,24,25] evaluating the dependence of the CO_2 adsorption reaction on the Li_4SiO_4 surface properties. Nevertheless, there are scarce studies on the structural, electronic, thermodynamic and CO_2 capture properties of these compounds, [26,27] especially for eutectic mixtures, which can be attained through theoretical studies. One of the eutectic mixtures that have attracted much attention in recent years is Li_2O-Na_2O-SiO_2 system, an important class of material not only for CO_2 adsorption[28,29] but also for glass,[30,31] mold-flux,[32,33] and steel industry.[34] The main reason is that Na-containing silicates are able to form eutectic melts with the Li_2CO_3 shell (one of the products of Li_4SiO_4 carbonation) at high temperatures, which favours the CO_2 diffusion through the product layer.[35] In this respect, some studies have reported the prevailing role of newly formed Li_3NaSiO_4 in improving the CO_2 sorption,[36,37,38] as well as its CO_2 sorption mechanism,[39] but the structural, electronic, thermodynamic and CO_2 capture properties of Li_3NaSiO_4 applying Density Functional Theory (DFT) calculations have not been studied.

Therefore, in this work, the structural, electronic, thermodynamic and CO_2 capture properties of monoclinic phases of Li_4SiO_4 and a binary (Li_3NaSiO_4) eutectic mixture were thoroughly investigated by using DFT calculations, considering (001), (010) and (100) surfaces. Kong et al. [40] studied low Miller index surfaces of Li_4SiO_4 visa First Principles calculations showing (010) plane as the most stable among low index ones, although with small differences for all the low index ones. Therefore, low index planes (010), (100) and (001) were selected in this work as the most symmetric options between the low index – low energy ones as representative surfaces for CO_2 adsorption.

The reported results allowed to analyse the properties of the eutectic mixture in comparison with the Li_4SiO_4 and the CO_2 properties at the interfaces of both silicates.

View Article Online
DOI: 10.1039/D2CP00346E

2. Methods

Electronic structure calculations for pure silicates and for the adsorption of CO_2 on Li_4SiO_4 and Li_3NaSiO_4 surfaces have been carried out using the software package SIESTA[41] (v4.1-b4). The Generalized Gradient Approximation (GGA) using the Perdew-Burke-Ernzerhof (PBE)[42] scheme was considered. Norm-conserving Troullier-Martins pseudopotentials[43] factorized in the Kleinman-Bylander form[44] with numerical Double zeta plus polarization orbitals (DZP) basis sets were used for all the calculations. An energy cutoff of 500 Ry was used. A *k*-point mesh of 3 × 5 × 5 using the Monkhorst-Pack grid was considered.[45] Tests for the selection of the number of *k*-points and energy cut-off were carried out (Tables S1 and S2, Supplementary Information), which led to the selection of the parameters used along this work. Structural relaxation using the Conjugated Gradient method was used, with 0.01 eV $Å^{-1}$ as convergence criteria for forces acting on each atom. Dispersion corrections were considered using Grimme's DFT-D3 method[46] for all the systems, additional corrections such as Becke-Johnson damping function[47] are not considered.

Li_4SiO_4 crystal is characterized by a monoclinic structure with a space group $P2_1/m$.[20] Li_4SiO_4 has another phase (γ-Li_4SiO_4) in triclinic structure with space group *P1*, although this γ phase appears at low temperature.[26] Therefore, the monoclinic structure was considered for all the Li_4SiO_4 calculations considered in this work in agreement with previous studies.[48] In the case of Li_3NaSiO_4, there is no crystallographic information, so for its characterization, a monoclinic structure with a space group $P2_1/m$ has also been considered in parallel to Li_4SiO_4. In the case of Li_4SiO_4, a crystal structure containing 126 atoms (14 formula units) was considered in agreement with the experimental data by Tranqui et al.[49] and previously used for DFT studies.[26,48] An analogous 126-atoms cell was considered for Li_3NaSiO_4, Fig. 1. The bulk structures for both silicates were fully relaxed and new cell parameters and atomic positions were inferred at the considered theoretical level. For developing surfaces, relaxed bulk crystals, Figure S1 (Supplementary Information), were cleaved along the (001), (010) and (100) Miller's planes. In this surface building procedure, a two-layers depth slab demonstrated to be thick enough to obtain consistent energies, while a (2 × 2) supercell reconstruction turned to be large enough to avoid interaction between the periodic images. For Li_4SiO_4

View Article Online
DOI: 10.1039/D2CP00346E

surfaces, considered systems contained 100 Li + 24 Si + 96 O (001), 63 Li + 14 Si + 56 O (010), and 58 Li + 16 Si + 64 O (100). For Li_3NaSiO_4 surfaces, 30 Li + 14 Na + 12 Si + 48 O (001), 40 Li + 14 Na + 14 Si + 56 O (010), and 42 Li + 14 Na + 16 Si + 64 O (100). These surfaces were fully relaxed, and after relaxation a single CO_2 molecule was placed on top of different surface positions, to analyse the different surface adsorption sites, Figure S2 (Supplementary Information). All the simulations were carried out using periodic boundary conditions in the three space directions. In the case of surfaces a vacuum layer 20 Å long was considered in the direction perpendicular to the surface to avoid interactions with neighbouring cells.

The CO_2 adsorption energy, E_{ads}, was calculated using the following formula:

$$E_{ads} = E_{surf+CO2} - E_{surf} - E_{CO2} \quad (1)$$

where $E_{surf+CO2}$ is the energy of the (relaxed) whole system, E_{surf}, the energy of the clean surface (relaxed in absence of CO_2) and E_{CO2} the energy for the isolated CO_2 (simulated as a single molecule in a 20×20×20 $Å^3$ box). In order to get insight into the nature of CO_2 adsorption on these silicates, we computed Hirshfeld[50] charges before and after adsorption of CO_2. In this way, it would be possible to identify any possible charge transfers between atoms, getting conclusions on the nature of the adsorption. Hirshfeld charges were used instead of Mulliken ones considering that Mulliken-charges are largely dependent on the applied basis set and they are not suitable when using diffuse orbitals[51] as the DZP ones considered in this work.

Further analysis of CO_2-lithium silicate systems was carried out using Ab initio molecular dynamics (AIMD) simulations for selected systems. The objective of AIMD simulation was to infer dynamic behavior of the systems in comparison with the so-called static calculations as well as to study the temperature effect on the CO_2 adsorption. The simulation boxes used for AIMD studies were the same ones as those used for the aforementioned calculations. AIMDs were carried out in the NVT ensemble at 1528 K (for Li_4SiO_4 systems) or 1050 K (for Li_3NaSiO_4), with the temperature controlled using the Nose thermostat (Nose mass = 100 Ry fs^2), with 1 fs time step, up to 1 ps total simulation time. The AIMD simulations were carried out at temperatures according to their melting points.[52,53]

View Article Online
DOI: 10.1039/D2CP00346E

3. Results and discussion

3.1 Properties of Li_4SiO_4 and Li_3NaSiO_4 bulk crystalline structures and interfaces.

The optimized monoclinic *P2₁/m* structure for Li_4SiO_4 is reported in Figure S1a (Supplementary Information). Results obtained in this work are in fair agreement with available experimental and computational studies (Supplementary Information). In the case of Li_3NaSiO_4, the absence of any experimental or computational results hinders any comparison with the results reported in this work. The Li_3NaSiO_4 optimized crystal structure is reported in Figure S1a (Supplementary Information), crystal cell parameters (*a,b,c*) are lower than those for Li_4SiO_4, leading to a cell volume 10 % lower, i.e. more compact cell. Nevertheless, the SiO_4 structure is not remarkably changed in Li_3NaSiO_4, as the Si-O bond distance is the same as in Li_4SiO_4 and only a smaller β angle is inferred. The electronic distribution reported in Figure S1b (Supplementary Information) is analogous to that in Li_4SiO_4. The main difference in the electronic properties stands on the DOS reported in Figure S1c (Supplementary Information), which leads to a direct band gap of 3.6 eV, which is lower than the value for Li_4SiO_4. Therefore, Li_3NaSiO_4 is a semi-conductive material and the presence of Na cations decreases the band gap. Literature results for Li_2O and Na_2O showed band gaps of 5.8 and 2.4 eV,[54] respectively, thus confirming the effect of sodium on the decrease of Li_3NaSiO_4 with regard to Li_4SiO_4.

The properties of Li_4SiO_4 and Li_3NaSiO_4 surfaces along the (001), (010) and (100) planes were also studied. The cell parameters are reported in Table 1 as well as the surface energy, E_{surf}, calculated using eq. 2:

$$E_{surf} = \left[E_{slab} - \left(\frac{N_{slab}}{N_{bulk}}\right)E_{bulk}\right]/2A_{slab} \qquad (2)$$

Where the subscript *slab* and *bulk*, stand for the properties of the systems with surfaces (Table 2) and for those of the bulk crystals (Figure S1, Supplementary Information), respectively. *E* stands for total energy, *N* for the number of atoms in the simulated cells, and *A* for the area of the surfaces. The E_{surf} values reported in Table 1 show that surfaces stability ordering are as follows (100) > (001) > (010), both for Li_4SiO_4 and Li_3NaSiO_4 surfaces. Kong et al.[40] reported stability ordering (010) > (100) > (001) calculated at GGA/PW91 in contrast wit GGA/PBE values in this work, with the differences being justified considering the different levels for calculations as well as the different performance of PW91 and PBE.[55] Nevertheless, the E_{surf} values obtained in this works

View Article Online
DOI: 10.1039/D2CP00346E

and in reasonable agreement with literature ones. The stability of Li_3NaSiO_4 surfaces is slightly larger than those for Li_4SiO_4, except for (010), the less stable surface. Nevertheless, E_{surf} values for Li_4SiO_4 and Li_3NaSiO_4 surfaces are very similar, thus showing minor effects on surface stability because of the presence of Na ions. Likewise, the (*a,b,c*) crystallographic parameters are also very similar for both lithium silicates, the slightly larger values for Li_3NaSiO_4 surfaces show a minor expansive effect because of the presence of the bulkiest sodium atoms. The electronic properties are analyzed through the electron density contour maps, Figure 1. The presence of high-density spots on the surface, in the vicinity of oxygen atoms, shows the sites for prevailing adsorption of CO_2 molecules. These concentration of charge sites are present for all the surfaces and both for Li_4SiO_4 and Li_3NaSiO_4.

3.2 CO_2 on Li_4SiO_4 and Li_3NaSiO_4 surfaces.

The adsorption of CO_2 on Li_4SiO_4 and Li_3NaSiO_4 surfaces was studied for (001), (010) and (100) surfaces considering a selection of different adsorption sites, P_i. The selection of adsorption sites was done considering the geometry of the surface, the possible different sites were inferred and the adsorption energy calculated for all of them. The structures before and after CO_2 adsorption are reported in Figures 2 and 3 for the different adsorption sites as well as geometric, charges and energy related parameters in Tables 2 and 3. The reported results for E_{ads}, Table 2, are remarkably large for all the silicates, surfaces and adsorption sites. These large E_{ads} values indicate strong chemisorption of CO_2 molecules for all the available adsorption sites, thus leading to a deformation and bending of CO_2 molecules on the lithium silicates surfaces. The E_{ads} values on Li_4SiO_4 surfaces indicate (0 0 1) (-9.8 eV) > (0 1 0) (-7.3 eV) > (1 0 0) (-3.2 eV). Therefore, (0 0 1) is clearly favored over other possible surfaces although the large value of E_{ads} for the three studied surfaces show chemical sorption for all of them. In the case of Li_3NaSiO_4 surfaces, values are lower than for Li_4SiO_4 (-7.2 eV in comparison with -9.8 eV, respectively for the stronger adsorption sites) and the surfaces ordering being (0 1 0) (-7.2 eV) >(1 0 0) (-6.9 eV) > (0 0 1) (-2.6 eV). Therefore the (0 0 1) is destabilized in terms of CO_2 adsorption on going from Li_4SiO_4 and Li_3NaSiO_4. Therefore, the introduction of Na atoms on the studied silicate surfaces led to a slight weakening of CO_2 adsorption. Nevertheless, the adsorption kinetics is improved by the doping, thus leading to two

View Article Online
DOI: 10.1039/D2CP00346E

opposite effects upon doping: adsorption weakening (thermodynamics) coupled with faster adsorption rates (kinetics). However, results in Table 2 confirm that CO_2 can be efficiently adsorbed for all the surfaces of both Li_4SiO_4 and Li_3NaSiO_4, which is of great relevance for CO_2 capturing purposes. Likewise, for a fixed surface (e.g. (0 0 1) Li_4SiO_4), results reported in Table 2 show non-negligible differences for E_{ads} when considering the different adsorption sites (e.g. 1 eV for (0 0 1) Li_4SiO_4 or 3.0 for (0 1 0) Li_4SiO_4).Therefore, preferential adsorption sites may be inferred, although small E_{ads} values are not reported for any of the considered adsorption sites, thus confirming that CO_2 molecules can be efficiently adsorbed at different sites on each surface, i.e. allowing large CO_2 capturing ability. The comparison of cell parameters for neat surfaces (in absence of CO_2, Table 1) with those upon CO_2 adsorption (Table 2) show that upon adsorption of this molecule, both the structural parameters of CO2 as from the surface are affected. Therefore, crystal cell evolving in response to the strong interaction with adsorbed molecules. These changes are in some cases cell expansions (e.g. (001) surfaces for both lithium silicates) and in other ones, cell contractions (e.g. (100) surfaces), which are responses to the strong CO_2 adsorption. These structural changes are also indicated by the adsorbed gas to surface distance reported in Table 2, these distances being in the 2 to 4.2 Å range, depending on the site and surface. The reduced Density Gradient (RDG) for the CO_2 molecule interacting with the surface (Figure 4) confirms strong interaction in the area on the surface below the gas molecule.

The effect of adsorbed CO_2 molecules on the electronic properties of the surfaces is analyzed through the DOS reported in Figure 5 for selected adsorption sites corresponding to the largest E_{ads} (Table 2). The DOSs show very minor changes upon CO_2 adsorption, and although the adsorption of CO_2 molecules leads to the modification of the electronic properties of lithium silicates because of the strong adsorption as reported by the large E_{ads} these effects are not remarkable.

Likewise, CO_2 molecules suffer large changes upon adsorption indicating chemical sorption. The changes in CO_2 properties are reported in Table 3. The C-O bond distances are elongated upon adsorption for all the considered sites and these elongations are larger for Li_4SiO_4 than for Li_3NaSiO_4 surfaces. The calculated C-O bond distance for isolated, not adsorbed, CO_2 molecules is 1.18 Å, with results in Table 3 indicating bonds elongated up to 1.50 Å, which is a sign of bond breaking for some

View Article Online
DOI: 10.1039/D2CP00346E

adsorption sites. Moreover, the large bending of CO_2 molecules, Figure 3, is quantified by the corresponding O-C-O angles, with values as low as 103° obtained for the stronger adsorption sites. Therefore, the large E_{ads} as well as the changes in the geometrical parameters of CO_2 molecules point to initial stages of breaking of CO_2 molecules in the lithium silicate surfaces. The possible charge transfer surface-CO_2 is analyzed through the Hirshfeld charge, Table 3. For isolated CO_2 molecule, gas phase, the Hirshfeld charge for the carbon atom is +0.218, whereas -0.109 was calculated for the oxygen atoms, thus neutral CO_2 molecule. Results in Table 3 show that upon adsorption non-neutral CO_2 molecules are formed in all the cases. The sign of the total charge for CO_2 depends on the nature of the adsorption site, with sites close to surface oxygen atoms leading to positively charged molecules whereas the reverse effect was inferred for sites closer to silicon atoms.

3.3 AIMD of CO_2 on Li_4SiO_4 and Li_3NaSiO_4 surfaces.

The results reported in the previous section allowed to confirm the chemical adsorption of CO_2 on the surfaces of the considered lithium silicates. The dynamics and temperature effect on this strong adsorption were studied by AIMD simulations at 1528 K (for Li_4SiO_4 systems) or 1050 K (for Li_3NaSiO_4). The AIMD evolution of a single CO_2 molecule adsorbed on the (010) surface of both silicates allowed to analyze relevant structural properties. Radial distribution functions, RDFs, for the center of mass of CO_2 molecules (C atom) and lithium silicate surface atoms are reported in Figure 6. In the case of Li_4SiO_4, Figure 6a, the reported RDFs show closer contacts between C atoms and Li ones, the first peak at 2.2 Å for C-Li RDFs indicates strong interactions with the Li cation. For the interaction with the silicate anions, RDFs for C-O pairs show lower distances than for C-Si ones, as the surfaces are rich in O atoms from the silicates, therefore leading to stronger interactions with the oxygen atoms. Nevertheless, the C-O peak appears at larger distances than C-Li ones, thus, stronger interactions with the cations than with the anions (O atoms) is inferred. This would justify the large negative charge for (010) surface as reported in Table 3, corresponding to the extraction of charge from lithium atoms. In the case of Li_3NaSiO_4, the reported RDFs, Figure 6b, are less defined than for Li_4SiO_4, with less intense peaks. The presence of Na atoms changes all the RDFs, C-Li and C-Na RDFs appear at roughly the same distance but increases when

View Article Online
DOI: 10.1039/D2CP00346E

compared with Li_4SiO_4, i.e. CO_2 molecules are pushed away of Li cations, when eutectic mixture is formed. On the contrary, C-O and C-Si decreases in the eutectic, with remarkably low C-O distances, which point to strong contacts of gas molecules with the silicates through the O atoms. Therefore, the mechanism of interaction with the surface is different in the Li_4SiO_4, prevailing contacts with surface lithium cations, in comparison with Li_3NaSiO_4, closer contacts with silicate anions through oxygen atoms.

The atomic distribution on the surfaces is analysed through the density profiles in the direction perpendicular to the surfaces, *z*, Figure 7. These density profiles confirm the peaking of density data for Li atoms at the surface in close contact with CO_2 molecules, whereas for the eutectic Na atoms are placed in inner regions not so close to the surface as lithium ones. Nevertheless, the formation of the eutectic changes the properties of the surfaces, especially for silicate anions, which leads to closer contact with CO_2 molecules, especially with the enrichment of O atoms from silicates in the vicinity of CO_2.

The large changes in CO_2 molecules upon adsorption are also analysed with AIMD simulations. The time evolution of bond distances and angles are reported in Figure 8. Although an oscillatory behaviour is inferred for all the properties and both for Li_4SiO_4 and Li_3NaSiO_4, the CO_2 bending and bond elongation is maintained in both surfaces at the studied temperatures, with larger deformations for Li_3NaSiO_4. Likewise, the time evolution of E_{ads} reported in Figure 9 confirms that CO_2 molecules remains strongly adsorbed on both surfaces and no desorption is inferred, which is due to the strong gas-surface affinity even at high temperatures. The oscillatory behavior of CO_2 geometrical properties as well as for E_{ads} show gas molecules diffusing on the lithium silicate surface although remaining close to the sorption positions. For this purpose, CO_2 diffusion on the surface was analyzed from mean square displacements, *msd*, reported in Figure 10. The reported *msd* show faster diffusion on Li_3NaSiO_4 than on Li_4SiO_4, which can be related with the behavior of RDFs in Figure 6, i.e. more localized adsorption for Li_4SiO_4. Nevertheless, the oscillatory behavior inferred for *msd in* both silicates shows how CO_2 molecules are moving around the localized adsorption sites without leaving these positions, and producing the oscillations in geometrical properties and E_{ads} reported in Figures 8 and 9. This is confirmed by the calculated self-diffusion coefficients on the surface planes, D_{xy}, obtained from *msd* and Einstein's equation, Figure 10, being 420 and

View Article Online
DOI: 10.1039/D2CP00346E

875 $Å^2$ ns^{-1}, for Li_4SiO_4 and Li_3NaSiO_4, respectively. Nevertheless, once CO_2 molecules are adsorbed on the lithium silicate surfaces, they move around the corresponding adsorption sites but remain around these sites as indicated by the trajectories reported in Figure 11, thus maintaining strong interaction with the surfaces, Figure 9. Therefore, the chemical sorption with the disruption of the molecular properties of the adsorbed gas molecules is maintained at the high temperatures considered for AIMD simulations, thus these lithium silicates can be used as high temperature sorbents for CO_2.

The theoretical results using both static and dynamic approaches probed CO_2 activation on both silicates surfaces as confirmed by: i) very large adsorption energies, ii) bending of CO_2 molecules, iii) elongation of C – O bonds, iv) charge transfer from sorbent to adsorbed gas molecules and v) efficient adsorption at high temperatures close to salts melting point. The CO_2 activation confirms chemisorption on the considered silicate surfaces for all they studied low Miller index surfaces and the suitability of the considered materials CO2 capture purposes.

4. Conclusions

The properties of lithium silicates for CO_2 capturing purposes are studied in this work using Density Functional Theory. The results show strong chemical adsorption of the different adsorption sites of all the available surfaces, both for Li_4SiO_4 and Li_3NaSiO_4 eutectic. The adsorption is characterized by deformation of adsorbed gas molecules leading to bonds elongation and molecular bending, indicating breaking of CO_2 molecules upon adsorption. The adsorption of CO_2 molecules also changes the properties of the adsorbed surfaces, geometrical and electronic, as a consequence of the great affinity for the gas molecules. In the case of Li_4SiO_4, close contacts with lithium ions is inferred, whereas for Li_3NaSiO_4 interactions with oxygen atoms of silicates are preferred. The adsorption is also characterized by charge transfer resulting in charged CO_2 molecules. Ab initio molecular dynamics simulations show that the adsorption is not largely disrupted by the considered high temperatures with the gas molecules not desorbed and being geometrically disrupted. The diffusion of adsorbed molecules is larger for Li_3NaSiO_4 than for Li_4SiO_4, but in both cases CO_2 molecules remain close to the sorption sites oscillating around the equilibrium positions. This study confirms the

View Article Online
DOI: 10.1039/D2CP00346E

suitability of these silicates for high temperature CO_2 adsorption based on the nanoscopic confirmation of the great affinity of both materials, in all their surfaces, for the gas as well as the activation of CO_2 molecules upon adsorption. The consideration of Li_3NaSiO_4 maintains the capturing ability in comparison with Li_4SiO_4 but at lower temperatures.

Acknowledgements

This work is part of the CO2MPRISE, "CO2absorbing Materials Project-RISE", a project that has received funding from the European Union's Horizon 2020 research and innovation programme, under the Marie Skłodowska-Curie Grant Agreement No 73487. We also acknowledge SCAYLE (Supercomputación Castilla y León, Spain) for providing supercomputing facilities. The statements made herein are solely the responsibility of the authors.

Supplementary information

Tables S1 and S2 (tests on the effect of *k*-points grid and energy cut-off on (0 0 1) Li_4SiO_4 surface energy; Figure S1 (properties and discussion for bulk systems). Figure S2 (definition in interaction sites on the considered surfaces);

View Article Online
DOI: 10.1039/D2CP00346E

Table 1

Properties of cells for clean surfaces (in absence of CO_2) for the indicated compounds. Values obtained for optimized structures.

compound	Miller's plane	cell parameters (a, b, c) / Å	cell parameters (α, β, γ) / °	surface energy / J m^{-2}
Li_4SiO_4	(001)	(21.301, 12.019, 17.692)	(90, 90, 90)	2.17
	(010)	(16.074, 10.651, 16.129)	(90, 90, 101.01)	3.09
	(100)	(12.019, 16.074, 18.259)	(90, 90, 90)	1.60
Li_3NaSiO_4	(001)	(21.439, 12.134, 17.252)	(90, 90, 92.31)	2.00
	(010)	(16.600, 11.439, 15.974)	(90, 90, 101.33)	3.87
	(100)	(12.134, 16.600, 18.854)	(90, 90, 90.26)	1.50

Table 2

Properties for Li_4SiO_4/Li_3NaSiO_4-CO_2 systems. Values obtained for optimized structures. Adsorption sites labelling as in Figures 3 and 4. E_{ads} stands for CO_2 adsorption energy calculated according to eq. 1. *d* stands for the distance between the center-of-mass of CO_2 (C atom) and the center-of-mass of the closest Li_4SiO_4/Li_3NaSiO_4 (Si atom). Values obtained for optimized structures.

compound	Miller's plane	site	E_{ads} / eV	cell parameters* (a, b, c, α, β, γ) / Å , °	*d* / Å
Li_4SiO_4	(001)	1	-8.832	(21.646, 11.962, 17.072, 89.564, 77.487, 89.354)	1.97
		2	-9.753	(21.475, 11.581, 17.186, 94.606, 76.578, 87.947)	3.25
		3	-8.846	(21.265, 11.402, 17.338, 81.277, 81.779, 96.729)	2.68
	(010)	1	-4.241	(15.694, 9.207, 16.465, 88.268, 87.909, 94.409)	4.18
		2	-7.249	(15.542, 8.872, 15.659, 86.893, 82.052, 89.704)	3.76
		3	-4.485	(15.650, 9.387, 15.319, 89.397, 90.466, 94.318)	2.11
		4	-4.202	(15.674, 9.340, 15.503, 86.540, 82.155, 94.311)	3.12
	(100)	1	-3.208	(11.329, 13.015, 20.261, 99.609, 91.567, 97.759)	3.46
		2	-2.994	(10.994, 13.118, 18.403, 88.191, 81.385, 87.636)	3.21
		3	-1.947	(11.309, 12.874, 18.272, 90.116, 89.137, 89.882)	3.35
Li_3NaSiO_4	(001)	1	-2.556	(11.518, 10.148, 14.254, 85.003, 97.424, 86.877)	3.65
		2	-1.336	(12.104, 10.138, 14.632, 83.140, 82.866, 85.690)	3.48
		3	-1.916	(11.596, 10.177, 16.300, 85.437, 89.572, 86.802)	3.19
		4	-1.929	(11.836, 9.957, 16.562, 81.820, 94.137, 86.318)	3.57
	(010)	1	-7.157	(16.732, 8.448, 13.935, 99.853, 85.635, 90.313)	2.89
		2	-3.624	(16.917, 8.559, 15.564, 99.440, 83.162, 90.619)	3.61
		3	-4.775	(17.161, 8.369, 14.856, 92.626, 81.089, 89.374)	2.94
	(100)	1	-6.907	(10.649, 15.715, 15.863, 98.993, 101.993, 85.311)	3.21
		2	-4.777	(10.533, 15.239, 16.995, 103.350, 94.217, 86.328)	3.56
		3	-5.378	(10.479, 15.229, 18.290, 98.864, 91.577, 85.302)	3.42
		4	-4.575	(10.571, 15.660, 16.487, 96.252, 91.668, 83.686)	3.04
		5	-5.384	(10.294, 15.685, 17.101, 94.869, 91.320, 82.926)	2.71
		6	-6.134	(10.482, 15.493, 18.321, 91.060, 90.989, 82.561)	2.66

View Article Online
DOI: 10.1039/D2CP00346E

Table 3

Properties of CO_2 molecule upon adsorption on Li_4SiO_4/Li_3NaSiO_4 surfaces. Adsorption sites labelling as in Figures 3 and 4. *d* and Φ stand for distance and angle, respectively, considering C, O1 and O2 as CO_2 atoms. *q* stands for atomic charges, calculated using Hirshfeld method. q_{CO2} stands for the total charge of CO_2 molecule upon adsorption.

compound	Miller's plane	site	$d_{C\text{-}O1\ (CO2)}$ / Å	$d_{C\text{-}O2\ (CO2)}$ / Å	$\Phi_{O1\text{-}C\text{-}O2\ (CO2)}$ / °	q_C	q_{O1}	q_{O2}	q_{CO2}
Li_4SiO_4	(001)	1	1.28	1.32	118.38	0.181	-0.098	-0.064	0.019
		2	1.39	1.44	103.52	0.143	-0.069	-0.174	-0.100
		3	1.26	1.26	128.40	0.294	-0.077	-0.068	0.149
	(010)	1	1.25	1.50	108.83	0.024	-0.150	-0.215	-0.341
		2	1.29	1.34	114.91	-0.026	-0.181	-0.199	-0.406
		3	1.26	1.33	115.71	0.110	-0.168	-0.201	-0.259
		4	1.25	1.44	111.19	-0.022	-0.123	-0.180	-0.325
	(100)	1	1.18	1.18	173.51	0.299	-0.010	-0.027	0.262
		2	1.17	1.18	176.80	0.314	-0.005	-0.006	0.303
		3	1.16	1.20	177.42	0.328	0.009	0.007	0.344
Li_3NaSiO_4	(001)	1	1.18	1.18	169.78	0.333	-0.011	0.016	0.338
		2	1.17	1.19	174.22	0.269	-0.066	-0.033	0.170
		3	1.17	1.18	170.25	0.301	-0.021	-0.043	0.237
		4	1.17	1.18	171.84	0.314	-0.009	-0.034	0.271
	(010)	1	1.24	1.30	123.95	0.237	-0.165	-0.187	-0.115
		2	1.17	1.18	169.49	0.292	-0.053	-0.011	0.228
		3	1.23	1.24	137.45	0.246	-0.168	-0.173	-0.095
	(100)	1	1.26	1.27	126.98	0.254	-0.184	-0.195	-0.125
		2	1.17	1.18	177.05	0.325	0.010	-0.002	0.333
		3	1.25	1.28	125.46	0.241	-0.165	-0.156	-0.080
		4	1.17	1.18	176.88	0.313	0.019	-0.038	0.294
		5	1.24	1.27	133.78	0.223	-0.192	-0.190	-0.159
		6	1.25	1.28	127.61	0.262	-0.153	-0.126	-0.017

View Article Online
DOI: 10.1039/D2CP00346E

Figure Captions.

Fig. 1 Electron density contour maps at selected surfaces of Li_4SO_4 and Li_3NaSO_4.

Fig. 2 Snapshots showing initial configurations for (a) Li_4SiO_4 + CO_2, and (b) Li_3NaSiO_4 + CO_2 systems used for DFT calculations. Structures considering different surfaces, as defined by the corresponding (*i j k*) Miller planes, and different positions for the adsorption of CO_2 molecules, defined by *Pi*. Color code: (red) CO_2, (pink) silicate ions, (yellow) Li^+, (orange) Na^+.

Fig. 3 Snapshots showing optimized configurations for (a) Li_4SiO_4 + CO_2, and (b) Li_3NaSiO_4 + CO_2 systems used for DFT calculations. Structures considering different surfaces, as defined by the corresponding (*i j k*) Miller planes, and different positions for the adsorption of CO_2 molecules, defined by *Pi*. Color code: (red) CO_2, (pink) silicate ions, (yellow) Li^+, (orange) Na^+.

Fig. 4 Reduced Density Gradient analysis in the region close to adsorbed CO_2 on (0 0 1) Li_4SiO_4 surface. Values are reported in the plane through CO_2 molecule.

Fig. 5 Density of states as a function of orbital energy, E-E_f, for (a) Li_4SiO_4 + CO_2 and (b) Li_3NaSiO_4 + CO_2 systems. Curves show values for isolated Li_4SiO_4 or Li_3NaSiO_4, isolated CO_2, and Li_4SiO_4 / Li_3NaSiO_4 + CO_2 systems.

Fig. 6 Site – site radial distribution functions, $g(r)$, for the reported atomic pairs from AIMD simulations of 1 CO_2 molecule on (a) (0 1 0) surface of Li_4SiO_4 (P2 site, Figure 2) and (b) (0 1 0) surface of Li_4SiO_4 (P1 site, Figure 2).

Fig. 7 Number density, ρ, in the direction perpendicular to the surface for the reported atoms from AIMD simulations of 1 CO_2 molecule on (a) (0 1 0) surface of Li_4SiO_4 (P2 site, Figure 3) and (b) (0 1 0) surface of Li_4SiO_4 (P1 site, Figure 3). Dashed lines show the highest position of each type of atom for reference purposes.

Fig. 8 Time evolution of relevant CO_2 geometric parameters (C- O bod distance, d, and O-C-O angle, Φ) from AIMD simulations of 1 CO_2 molecule on (a,c) (0 1 0) surface of Li_4SiO_4 (P2 site, Figure 3) and (b,d) (0 1 0) surface of Li_4SiO_4 (P1 site, Figure 3).

Fig. 9 Time evolution of adsorption energy, E_{ads}, from AIMD simulations of 1 CO_2 molecule on (a) (0 1 0) surface of Li_4SiO_4 (P2 site, Figure 3) and (b) (0 1 0) surface of Li_4SiO_4 (P1 site, Figure 3). Dashed lines show E_{ads} from Table 2.

Fig. 10 Mean square displacement on *xy* plane (surface) for CO_2 center-of-mass, *msd*, from AIMD simulations of 1 CO_2 molecule on (0 1 0) surface of Li_4SiO_4 (P2 site, Figure 3) and (0 1 0) surface of Li_4SiO_4 (P1 site, Figure 3).

View Article Online
DOI: 10.1039/D2CP00346E

Fig. 11 Trajectory (red lines) on *xy* plane (surface) for CO_2 center-of-mass, from AIMD simulations of 1 CO_2 molecule on (0 1 0) surface of Li_4SiO_4 (P2 site, Figure 3) and (0 1 0) surface of Li_4SiO_4 (P1 site, Figure 3). Blue spheres show the initial ubication of the molecule on each adsorption site.

View Article Online
DOI: 10.1039/D2CP00346E

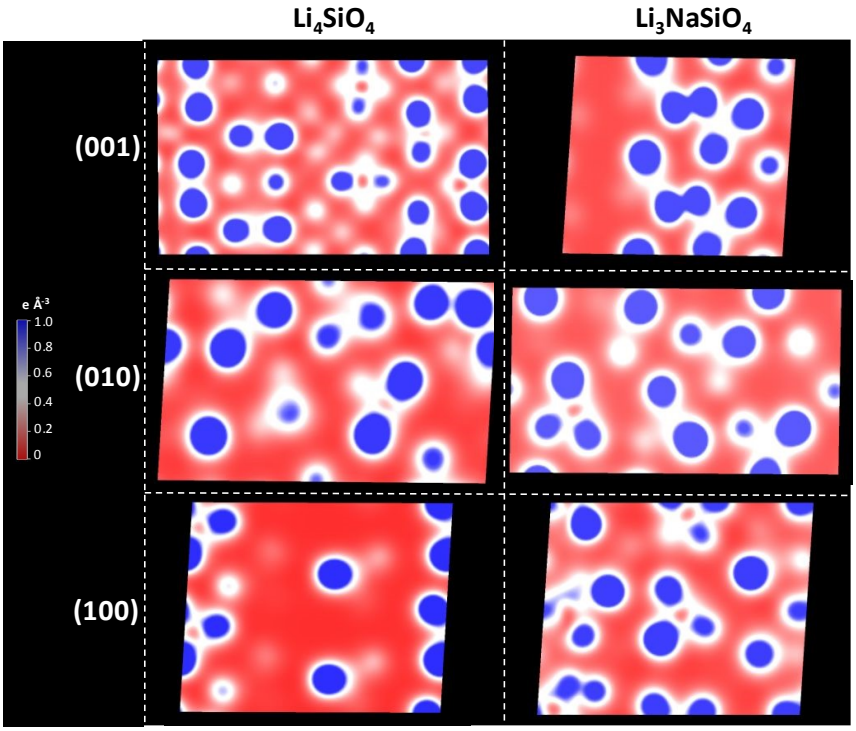

Fig. 1

View Article Online
DOI: 10.1039/D2CP00346E

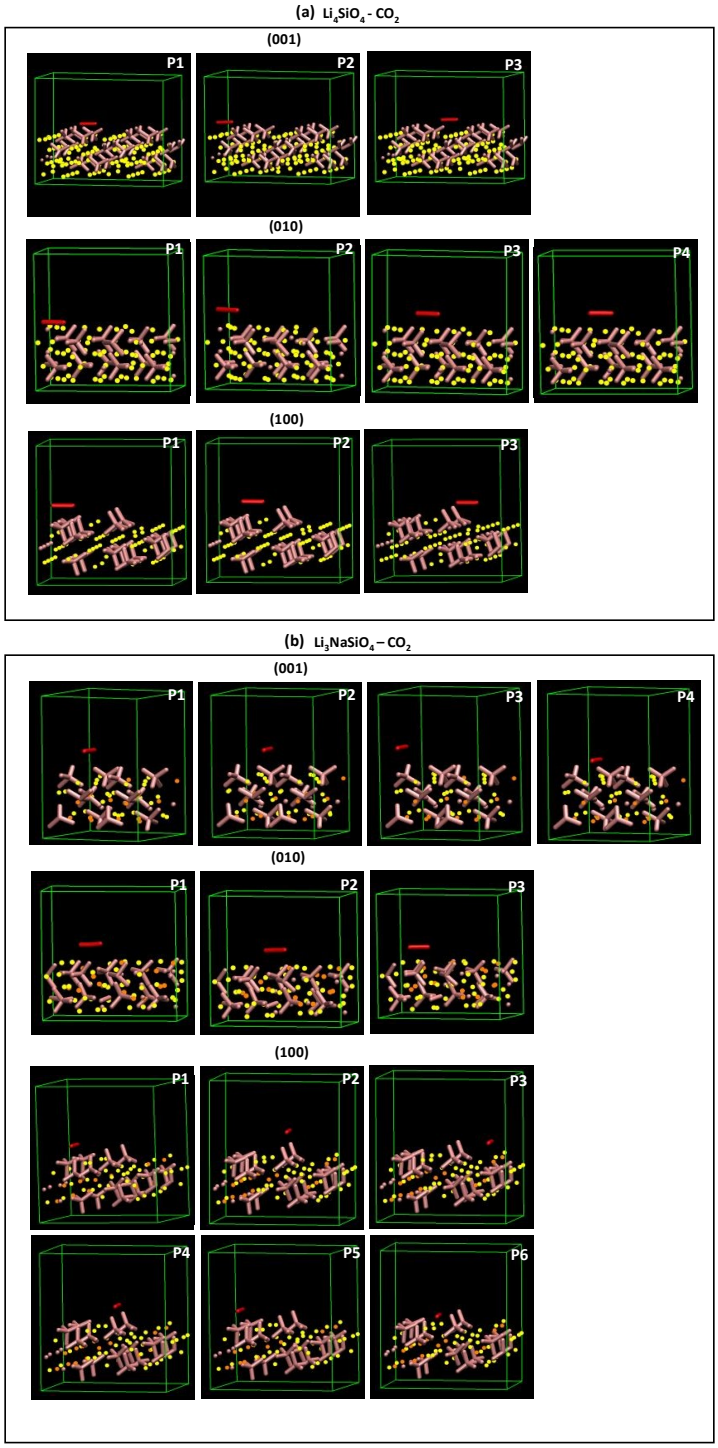

Fig. 2

View Article Online
DOI: 10.1039/D2CP00346E

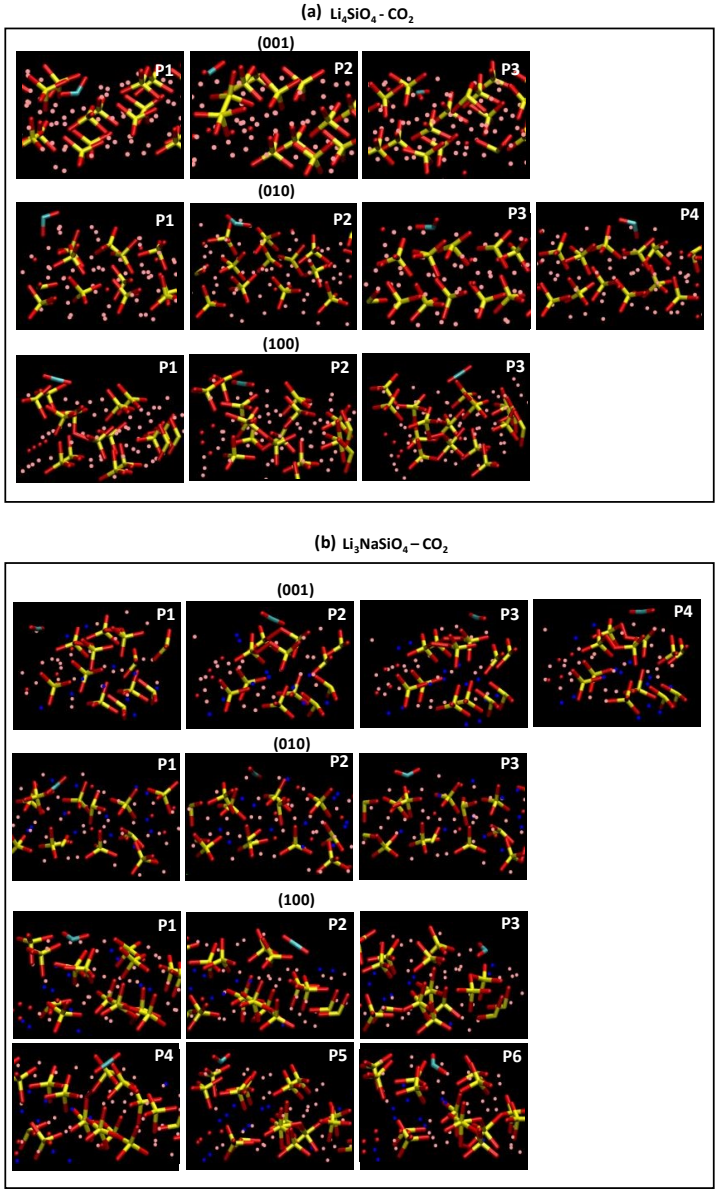

Fig. 3

View Article Online
DOI: 10.1039/D2CP00346E

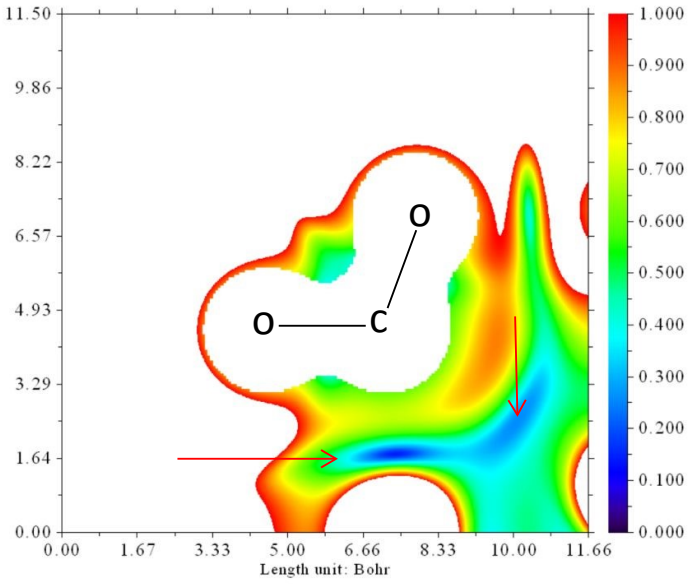

Fig. 4

View Article Online
DOI: 10.1039/D2CP00346E

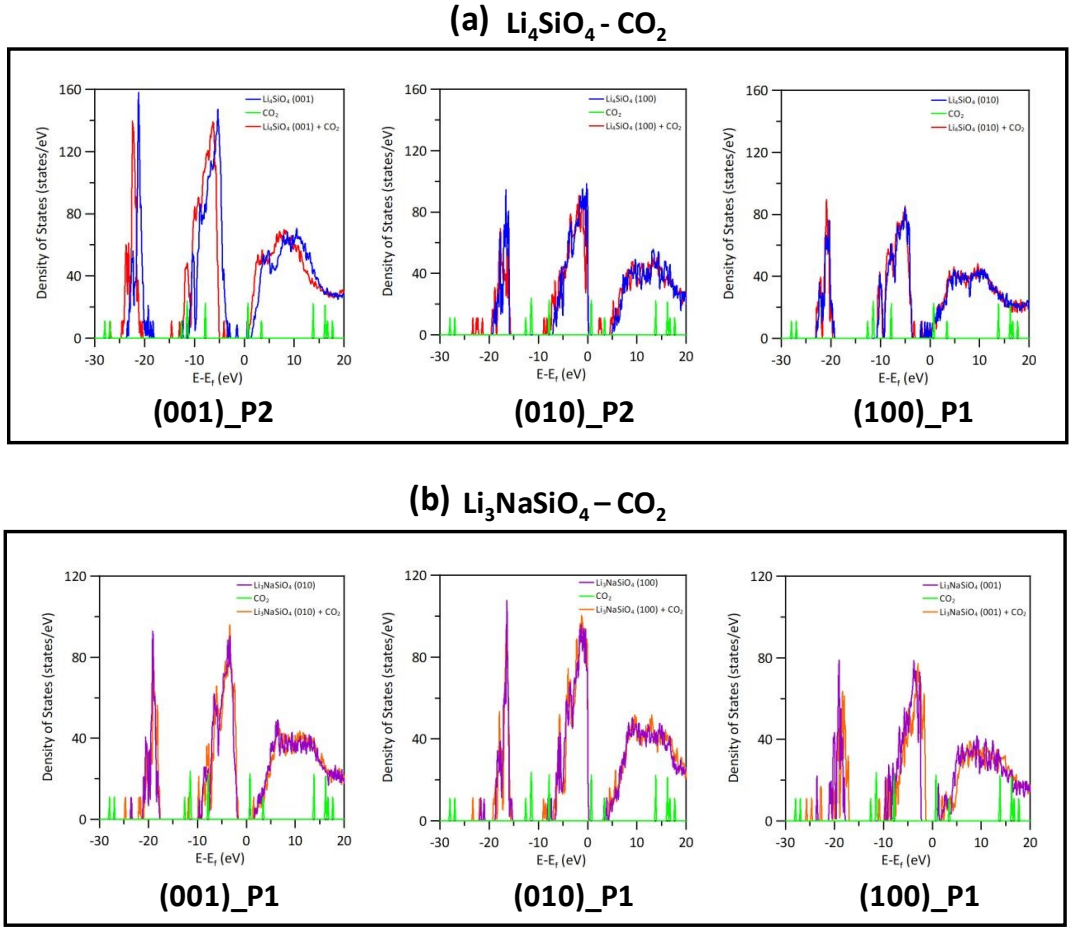

Fig. 5

View Article Online
DOI: 10.1039/D2CP00346E

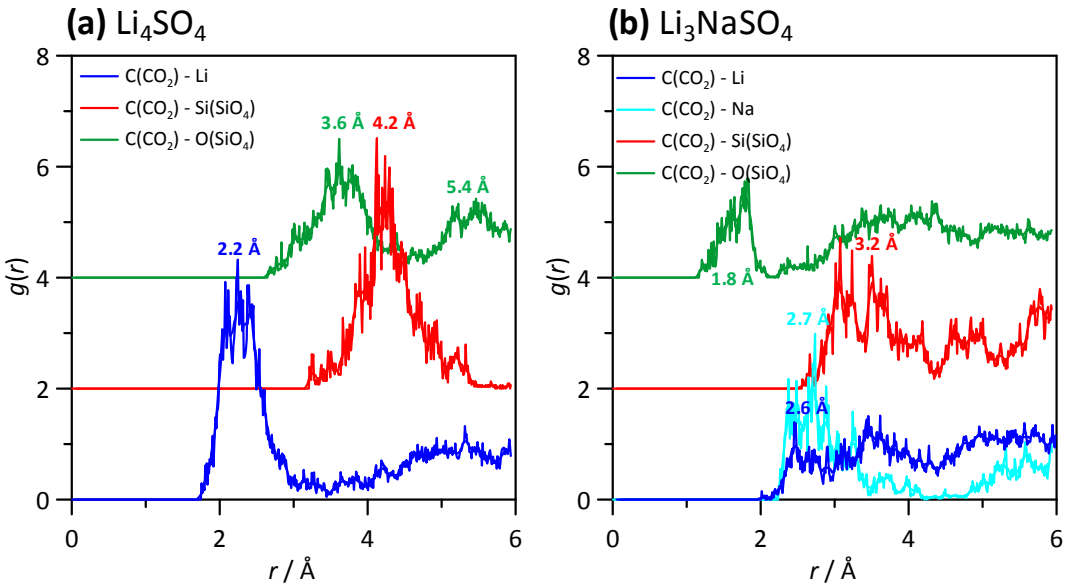

Fig. 6

View Article Online
DOI: 10.1039/D2CP00346E

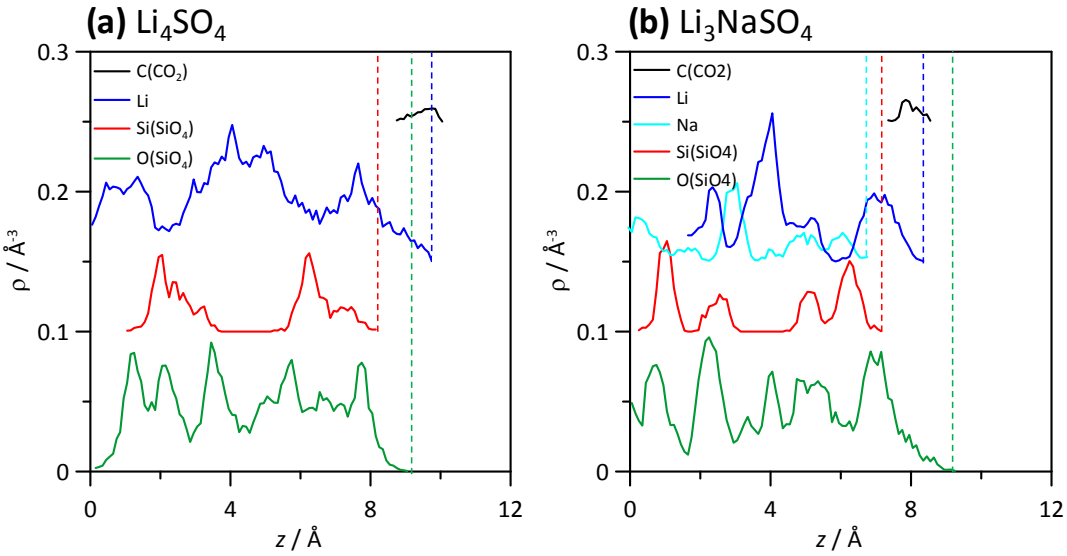

Fig. 7

View Article Online
DOI: 10.1039/D2CP00346E

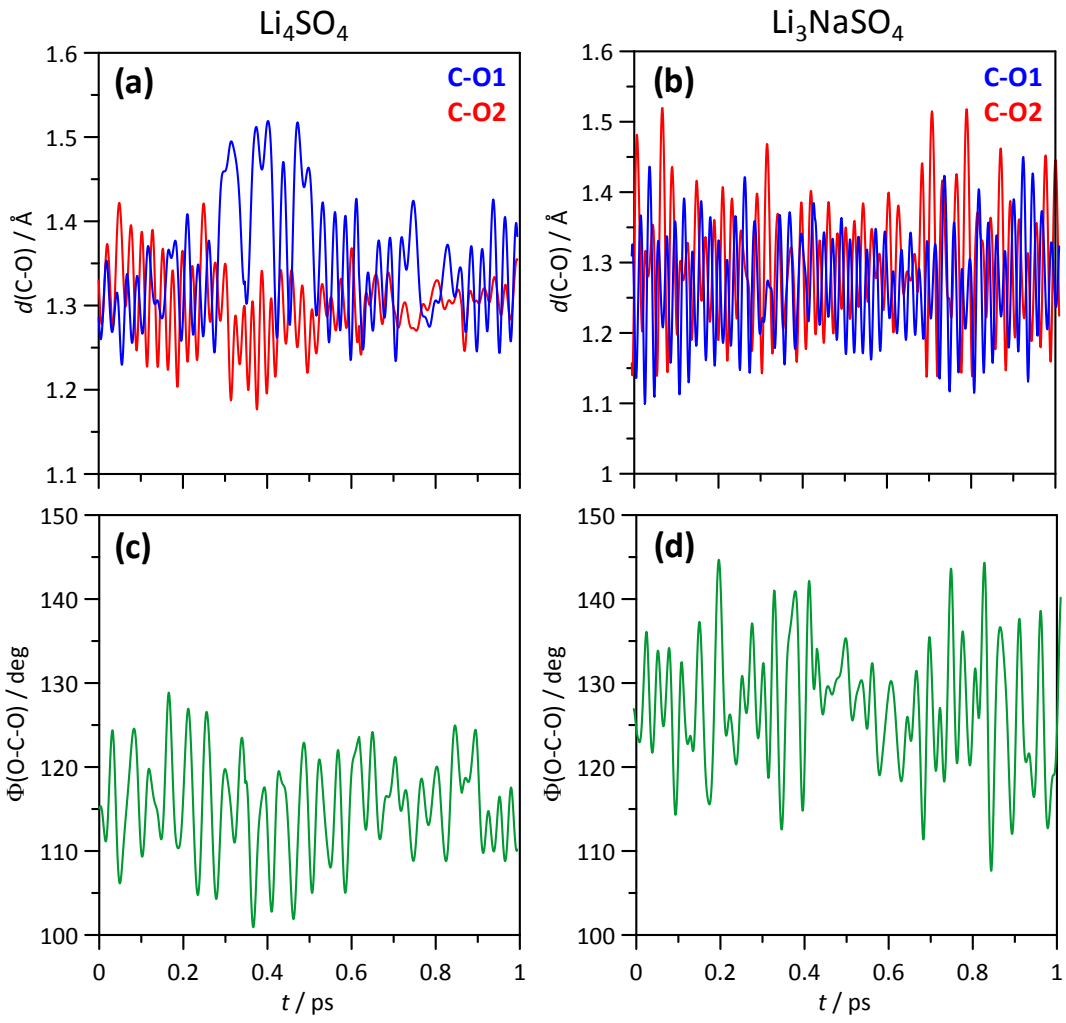

Fig. 8

View Article Online
DOI: 10.1039/D2CP00346E

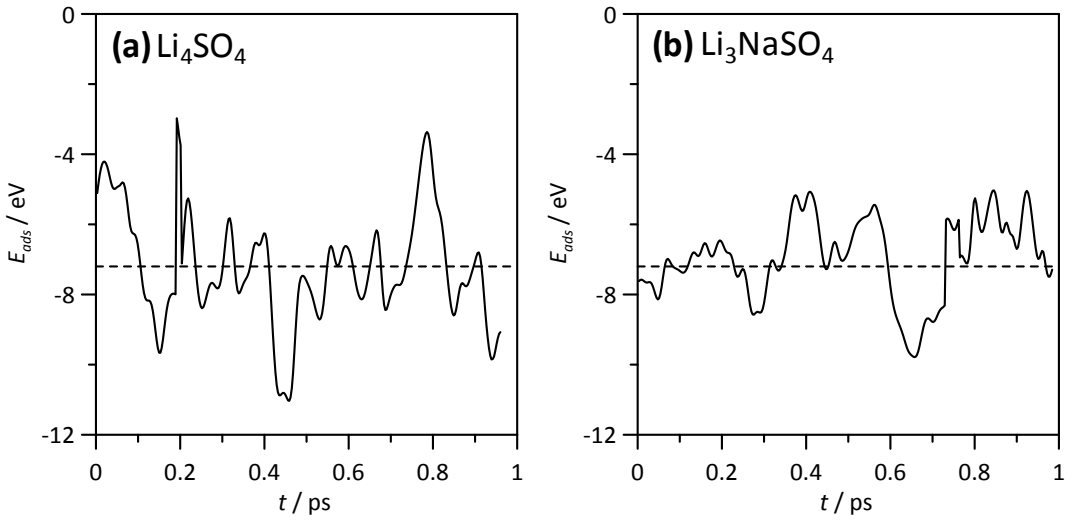

Fig. 9

View Article Online
DOI: 10.1039/D2CP00346E

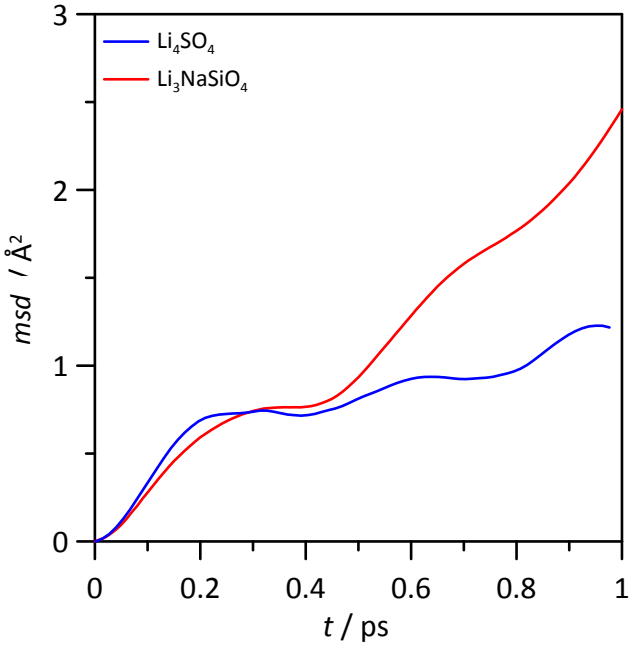

Fig. 10

View Article Online
DOI: 10.1039/D2CP00346E

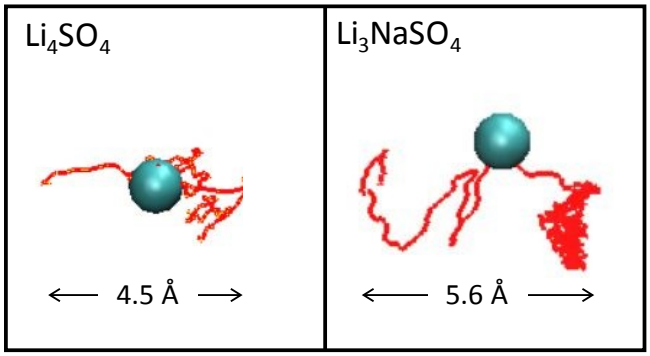

Fig. 11

View Article Online
DOI: 10.1039/D2CP00346E

References

1 Trends in Atmospheric Carbon Dioxide. https://www.esrl.noaa.gov/gmd/ccgg/trends/monthly.html (accessed January, 20, 2022).
2 C. Le Quéré, et al, *Earth Syst. Sci. Data,* 2018, **10**, 2141-2194.
3 E. I. Koytsoumpa, C. Bergins, E. Kakaras, *J. Supercrit. Fluids,* 2018, **132**, 3-16.
4 D. Bhattacharyya, D.C. Miller, *Curr. Opin. Chem. Eng.,* 2017, **17**, 78-92.
5 C. Zhang, J. Zhang, Z. Zhang, G.G.X. Wang, *Comput. Theor. Chem.* 2021, **1205**, 113424.
6 N.Y. Dzade, N.H. DE Leeuw, *Catalysts* 2021, **11**, 127.
7 R. Khaledialidusti, A. K. Mishra, A. Barnoush, *ACS Omega*, 2019, **4**, 15935-15946.
8 J. Wang, L. Huang, R. Yang, Z. Zhang, J. Wu, Y. Gao, Q. Wang, D. O'Hare, Z. Zhong, *Energy Environ. Sci*., 2014, **7**, 3478-3518.
9 J. Ida, Y. Lin, *Environ. Sci. Technol.,* 2003, **37**, 1999-2004.
10 Y. Hu, W. Liu, J. Sun, M. Li, X. Yang, Y. Zhang, X. Liu, M. Xu, *Fuel* 2016, 167, 17-24.
11 J. Sun, W. Liu, Y. Hu, M. Li, X. Yang, Y. Zhang, M. Xu, *Energy Fuel,* 2015, **29**, 6636-6644.
12 M. T. Izquierdo, V. Gasquet, E. Sansom, M. Ojeda, S. García, M. M. Maroto-Valer, *Fuel*, 2018, **230**, 45-51.
13 X. Yang, W. Liu, J. Sun, Y. Hu, W. Wang, H. Chen, Y. Zhang, X. Li, M. Xu, *ChemSusChem,* 2016, **9**, 2480-2487.
14 S. Zhang, Z. Qi, H. Wang, Y. Ni, Z. Zhu, *Int. J. Hydrogen Energy,* 2014, **39**, 17913-17920.
15 J. Ida, Y. Lin, *Environ. Sci. Technol.,* 2003, **37**, 1999-2004.
16 M. Kato, K. Nakagawa, K. Essaki, Y. Maezawa, S. Takeda, R. Kogo, Y. Hagiwara, *Int. J. Appl. Ceram. Technol.,* 2005, **2**, 467-475.
17 Y. Hu, W. Liu, Y. Yang, X. Tong, Q. Chen, *Z. Zhou, Ceram. Int.,* 2018, **44**, 16668-16677.
18 K. Wang, Z. Zhou, P. Zhao, Z. Yin, Z. Su, *J. Sun, Appl. Energy,* 2017, **204**, 403-412.
19 S. Zhang, Q. Zhang, H. Wang, Y. Ni, Z. Zhu, *Int. J. Hydrogen Energy,* 2014, **39**, 17913-17920.
20 M. Seggiani, M. Puccini, S. Vitolo, *Int. J. Greenh. Gas Con.,* 2013, 17, 25-31.
21 J. Ortiz-Landeros, I. C. Romero-Ibarra, C. Gómez-Yáñez, E. Lima, H. Pfeiffer, *J. Phys. Chem. C,* 2013, **117**, 6303-6311.
22 C. Gauer, W. Heschel, *J. Mater. Sci.,* 2006, **41**, 2405-2409.
23 M. Kato, S. Yoshikawa, K. Nakagawa, *J. Mater. Sci. Lett.,* 2002, **21**, 485-487.
24 K. Kanki, H. Maki, M. Mizuhata, *Int. J. Hydrog. Energy,* 2016, **41**, 18893-18899.
25 S. Zhang, Q. Zhang, H. Wang, Y. Ni, Z. Zhu, *Int. J. Hydrog. Energy,* 2014, **39**, 17913-17920.
26 Y. Duan, K. Parlinski, *Phys. Rev. B: Condens. Matter.,* 2011, **84**, 104113-1, 104113-10.
27 Y. Duan, H. Pfeiffer, B. Li, I. C. Romero-Ibarra, D. C. Sorescu, D. R. Luebke, J. W. Halley, *Phys. Chem. Chem. Phys.,* 2013, **15**, 13538-13558.
28 M. Kato, K. Nakagawa, K. Essaki, Y. Maezawa, S. Takeda, R. Kogo, Y. Hagiwara, *Int. J. Appl. Ceram.* Technol., 2005, **2**, 467-475.
29 A. Sanna, I. Ramli, M.M. Maroto-Valer, *Energy Procedia,* 2014, **63**, 739-744.
30 L.S. Gallo, T. De Marchi Mosca, B.H. Teider, I. Polyakova, A.C.M. Rodrigues, E.D. Zanotto, V.M. Fokin, *J. Non-Cryst. Solids,* 2015, **408**, 102-114.
31 V.M. Fokin, E.D. Zanotto, N.S. Yuritsyn, J.W.P. Schmelzer, J. Non-Cryst. Solids, 2006, **352**, 2681-2714.
32 M. D. Seo, C. B. Shi, J. W. Cho, S. H. Kim, *Metall. Mater. Trans. B,* 2014, **45**, 1874-1886.
33 H. Park, H. Kim, I. Sohn, *Mater. Trans B,* 2011, **42**, 324-330.
34 B. Lu, K. Chen, W. Wang, B. Jiang, Metall. Mater. Trans B, 2014, **45**, 1496-1509.
35 X. Yang, W. Liu, J. Sun, Y. Hu, W. Wang, H. Chen, Y. Zhang, X. Li, M. Xu, *ChemSusChem,* 2016, **9**, 2480-2487.
36 Y. M. Kwon, S. C. Lee, H. J. Chae, M. S. Cho, Y. K. Park, H. M. Seo, J. C. Kim, *Renew. Energy,* 2019, **144**, 180-187.
37 H. Cui, X. Li, H. Chen, X. Gu, Z. Cheng, Z. Zhou, *Energy,* 2019, **144**, 180-187.
38 I. Yanase, K. Sato, Y. Midorikawa, H. Kobayashi, T. Doe, T. Naka, *Mater. Lett.,* 2019, **238**, 93-97.
39 H. Cui, X. Li, H. Chen, X. Gu, Z. Cheng, Z. Zhou, *Chem. Eng. J.,* 2020, **382**, 122807-1, 122807-10.
40 X. Kong, Y. Yu, s. Ma, T. Gao, C. Xiao, X. Chen., *Chem. Phys. Lett.* 2018, **691**, 1-7.
41 J. M. Soler, E. Artacho, J. D. Gale, A. García, J. Junquera, P. Ordejón, D. Sánchez-Portal, *J. Phys.: Condens. Matter.,* 2002, **14**, 2745-2779.
42 J. Perdew, K. Burke, M. Ernzerhof, Phys. *Review Letters.,* 1966, **77**, 3865-3868.

View Article Online
DOI: 10.1039/D2CP00346E

43 N. Troullier, J. L. Martins, *Phys. Rev. B,* 1991, **43**, 1993-2006.
44 L. Kleinman, D. M. Bylander, *Phys. Rev. Lett.,* 1982, **48**, 1425-1428.
45 H. J. Monkhorst, J. D. Pack, *Phys. Rev. B: Solid State,* 1976, **13**, 5188-5192.
46 S. Grimme, J. Antony, S. Ehrlich, H. Krieg, *J. Chem. Phys.,* 2010, **132**, 154104.
47 S. Grimme, S. Ehrlich, L. Goerigk, *J. Comput. Chem.,* 2011, **32**, 1456-1465.
48 Y. Tang, P. Chen, W. Luo, D. Luo, Y. Wang, *J. Nuclear Mat*., 2012, **420**, 31-38.
49 D. Tranqui, R.D. Shannon, H.-Y. Chen, *Acta Cryst. B,* 1979, **35**, 2479-2487.
50 F. L. Hirshfeld, *Theoret. Chim. Acta,* 1977, **44**, 129-138.
51 R. Carbo-Dorca, *J. Matemat. Chem.,* 2004, **36**, 231-239.
52 S. Claus, H. Kleykamp, W. Smykatz-Kloss, *J. Nuclear Mat.,* 1986, **230**, 8-11.
53 B. Konar, P. Hudon, I.H. Jung, *J. Eur. Ceram. Society,* 2018, **38**, 2074-2089.
54 R.D. Eithiraj, G. Jaiganesh, G. Kalpana, *Physica B,* 2007, **396**, 124-131.
55 M. Fishman, H.L. Zhuang, K. Mathew, W. Dirschka, R.G. Hennig, *Phys. Rev.* B 2013, **87**, 245402.